



Contents lists available at ScienceDirect

European Journal of Medicinal Chemistry

journal homepage: <http://www.elsevier.com/locate/ejmech>

Identification of methyl (5-(6-((4-(methylsulfonyl)piperazin-1-yl)methyl)-4-morpholinopyrrolo[2,1-f][1,2,4]triazin-2-yl)-4-(trifluoromethyl)pyridin-2-yl)carbamate (CYH33) as an orally bioavailable, highly potent, PI3K alpha inhibitor for the treatment of advanced solid tumors

Hao-Yue Xiang^{a, b}, Xiang Wang^c, Yan-Hong Chen^a, Xi Zhang^c, Cun Tan^a, Yi Wang^c, Yi Su^c, Zhi-Wei Gao^d, Xiao-Yan Chen^d, Bing Xiong^a, Zhao-Bing Gao^e, Yi Chen^c, Jian Ding^{a, c, f, ***}, Ling-Hua Meng^{c, **}, Chun-Hao Yang^{a, *}

^a State Key Laboratory of Drug Research, Shanghai Institute of Materia Medica, Chinese Academy of Sciences, Shanghai, 201203, PR China

^b College of Chemistry and Chemical Engineering, Central South University, Changsha, 410083, PR China

^c Division of Anti-tumor Pharmacology, Shanghai Institute of Materia Medica, Chinese Academy of Sciences, Shanghai, 201203, PR China

^d Center for Drug Metabolism Research, Shanghai Institute of Materia Medica, Chinese Academy of Sciences, Shanghai, 201203, PR China

^e Key Laboratory of Receptor Research, Shanghai Institute of Materia Medica, Chinese Academy of Sciences, Shanghai, 201203, PR China

^f Shanghai HaiHe Pharmaceutical Co. Ltd., Shanghai, 201203, PR China

ARTICLE INFO

Article history:

Received 24 July 2020

Received in revised form

15 September 2020

Accepted 3 October 2020

Available online xxx

Keywords:

PI3K

Pyrrolo[2,1-f][1,2,4]triazine

Anti-cancer

Target therapy

ABSTRACT

In various human cancers, PI3Ks pathway is ubiquitously dysregulated and thus become a promising anti-cancer target. To discover new potent and selective PI3K inhibitors as potential anticancer drugs, new pyrrolo[2,1-f][1,2,4]triazines were designed, leading to the discovery of compound **37** (CYH33), a selective PI3K α inhibitor (IC₅₀ = 5.9 nM, β/α , δ/α , γ/α = 101-, 13-, 38-fold). Western blot analysis confirmed that compound **37** could inhibit phosphorylation of AKT in human cancer cells to modulate the cellular PI3K/AKT/mTOR pathway. And further evaluation *in vivo* against SKOV-3 xenograft models demonstrated that a dose-dependent antitumor efficacy was achieved.

© 2020 Elsevier Masson SAS. All rights reserved.

1. Introduction

Phosphatidylinositol 3-kinases (PI3Ks), as a kind of lipid kinases, play a vital role in cell survival and proliferation [1,2]. Class I PI3Ks is one of the most subtype of PI3K which catalyzes the conversion of PIP2 to a potent secondary messenger PIP3 that can recruit several proteins with pleckstrin homology domain to plasma membrane,

including AKT. Further phosphorylation of AKT stimulates mTORC1 through a signal transduction cascade [3,4]. There are accumulating evidence indicating that dysregulation of PI3K pathway is frequently encountered in various tumors [5,6]. The most common mechanisms associated with the activation of PI3K signaling are the mutation or amplification of PIK3CA gene [7,8]. Therefore, the inhibition of PI3K α was regarded as an efficient approach for treating cancer [9–13].

The importance of selectively inhibiting PI3K α in the treatment of cancer has already been well demonstrated in 2019 with the approval of the PI3K α inhibitor alpelisib (BYL719) [14]. Additionally, several PI3K α inhibitors, such as serabelisib (MLN1117) [15] and GDC-0326 [16], are also in preclinical or clinical trials (Fig. 1). Despite various PI3K inhibitors have been discovered, [17], [-26] due to the huge structure similarity of the ATP binding site between

* Corresponding author.

** Corresponding author.

*** Corresponding author. State Key Laboratory of Drug Research, Shanghai Institute of Materia Medica, Chinese Academy of Sciences, Shanghai, 201203, PR China.

E-mail addresses: jdj@sim.ac.cn (J. Ding), lhmeng@sim.ac.cn (L.-H. Meng), chyang@sim.ac.cn (C.-H. Yang).

PI3K isoforms, developing selective inhibitors still remains challenging.

Recently, a number of PI3K inhibitors were reported, and most of them shared similar structural and chemical features, including a central heterocycle substituted by one morpholine moiety and an aromatic cycle bearing a hydrogen bond donor group [27]. In our earlier research to identify novel inhibitors of this pathway, by virtue of the strategy of scaffold hopping from **PI-103** [28], we discovered compound **1**, which was found to hold a parallel potency against PI3K α and showed cytotoxicity at micromolar concentration [29]. However, the poor pharmacokinetic (PK) profile including poor solubility and rapid metabolism of compound **1** precluded its development. To address these issues, we herein identified a series of pyrrolo[2,1-*f*][1,2,4]triazines as PI3K inhibitors, culminating in the discovery of drug candidate **37** (**CYH33**). This study was focused to illustrate the discovery, molecular mechanism, pharmacodynamics and pharmacokinetics of **CYH33**, a clinical candidate currently in phase Ib clinical trial in China.

2. Results and discussion

2.1. Strategy for designing new PI3K inhibitors

Based on our previous work, we realized that the tricyclic core of compound **1** would be the inherent obstacle for its poor pharmacokinetic profile. Initially, a scaffold contraction strategy was adopted by replacing the tricyclic core of **1** with pyrrolo[2,1-*f*][1,2,4]triazine. Further inspired by the reported PI3K inhibitors [30–34] such as **GDC-0941**, **GNE-477**, and ETP-46321 and ETP-47037, the 4-methanesulfonyl-piperazin-1-ylmethyl group fragment segment was introduced designedly. It was found that the piperazine segment of **GDC-0941** can extend to the solvent-accessible region and form hydrogen bonds between the oxygens and the side chain of Ala805 and Lys802. Additionally, the existence of sulfonyl group can enhance its solubility. As a consequence, considering the benefit of piperazine group for PI3K inhibitory activity, this optimized segment was retained during the whole process of modification. Furthermore, the easily metabolized 3-hydrophenyl segment was optimized to improve the PK profile. As is well known, numerous drugs were incorporated fluorine-containing group into the molecules to improve the physicochemical properties and potency, [35], [36] which also be proved in the development of PI3K inhibitor such as **BKM-120** [37] and **PQR309** [38]. Analogously, the CF₃-containing 2-amino pyridine segment was incorporated into the pyrrolo[2,1-*f*][1,2,4]triazine

core, leading to a new PI3K inhibitor drug candidate compound **37** (Scheme 1).

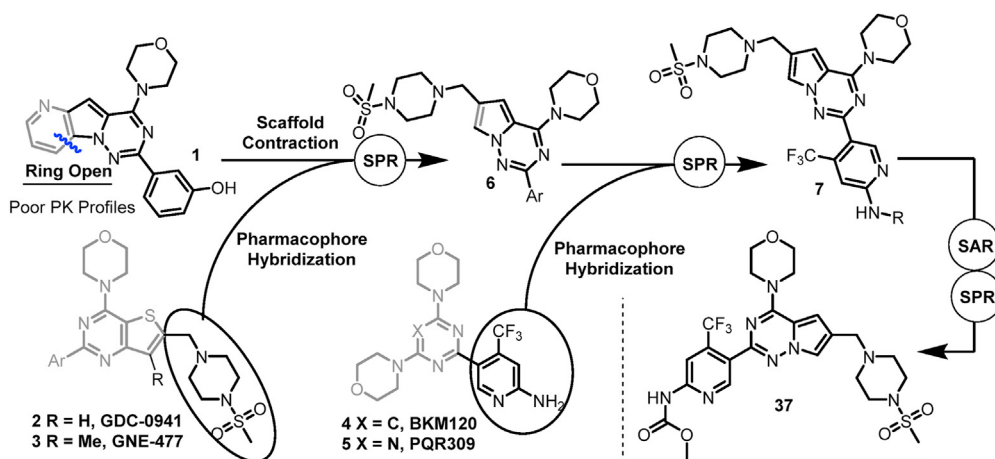
2.2. Preparation of target compounds

The key intermediate compound **11** was prepared from commercially available *p*-nitrobenzaldehyde and compound **10** according to the literature procedures reported by our group (Scheme 2) [39]. Chlorination of compound **11**, followed by amination with morpholine gave compound **13**. Reduction of the NO₂ group of compound **13** gave compound **14**. Hydrolysis of the resulting compound **14** afforded carboxylic acid derivative **15**, which could be condensed with 1-(methylsulfonyl)piperazine to furnish compound **16**. Following that, the compound **17** was obtained by reduction of the amide bond of compound **16** using BH₃·SMe₂ and then reacted with appropriate isocyanate, providing the corresponding urea derivatives **18–19**. Urea **19** could be further converted to compounds **21–23** by corresponding hydrolysis and condensation reaction. It is worth noting that the 4-(trifluoromethyl)pyridin-2-amine substituted analogues **28–38** (Scheme 3) were prepared similarly to **17–23** from the corresponding aldehyde.

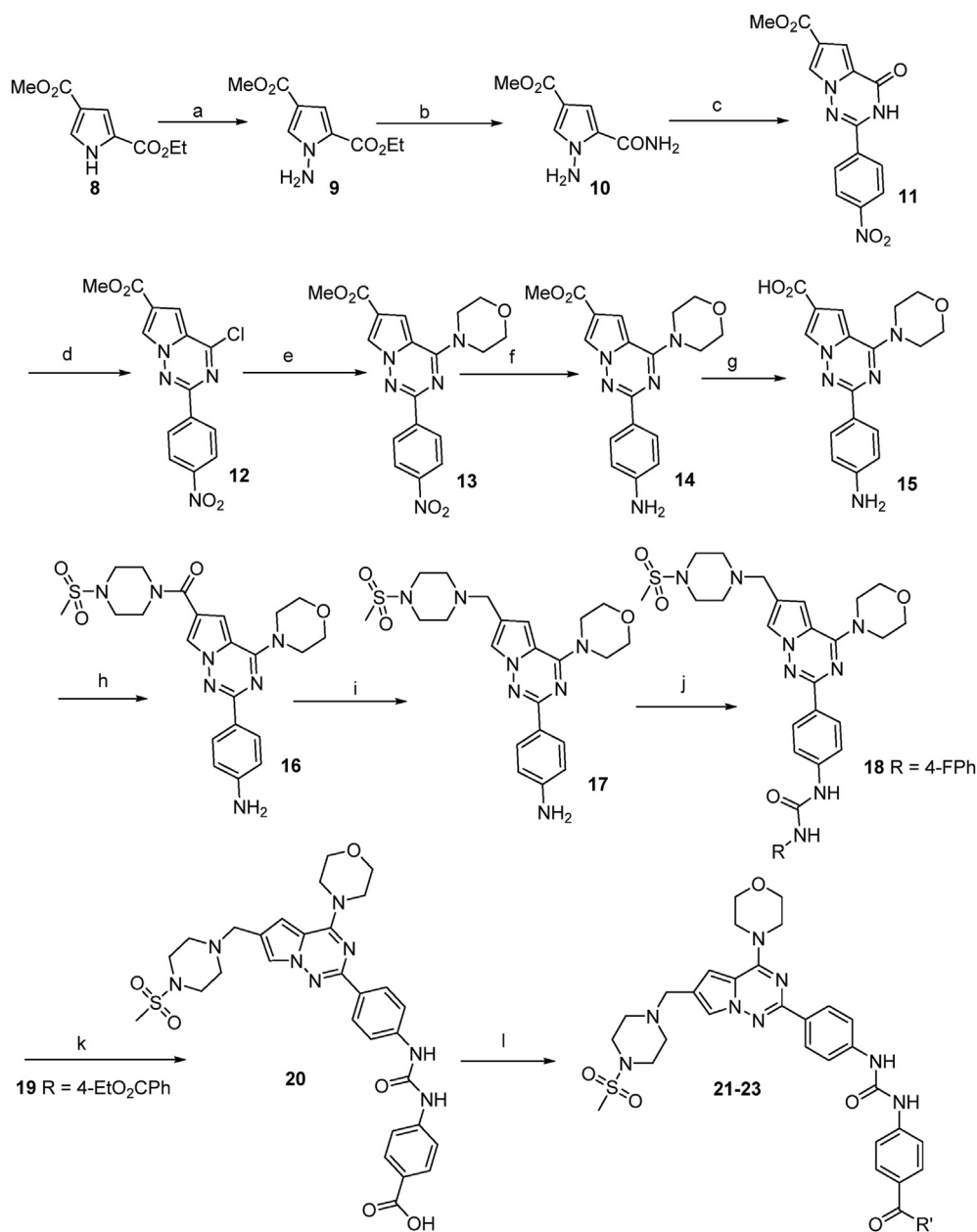
2.3. The cytotoxicity and PI3K α inhibitory activity

Our initial optimization was concentrated on the modification of amino groups on benzene ring, with the primary aim of keeping potency. As an early exploration, compounds **18–23** were prepared. To our delight, as shown in Table 1, compounds **21–23** exhibited favorable activity both at the enzymatic and cellular level. With these encouraging outcomes, compounds **18** and **22** were selected for further cytotoxic evaluation of 9 NSCLC cell lines. As shown in Table 2, compound **22** as well as **18** exhibited more potent anti-proliferative activity than **GDC-0941**. However, the pharmacokinetic profile of the two potent inhibitors **21** and **22** was quite disappointing (Summarized in Table S1 in SI). The oral bioavailability of compound **21/22** was only 0.2%/0.3% respectively, which may be due to their relative high molecular weight (>500), total polar surface area (tPSA>140), and poor solubility. Consequently, we continued to concentrate on improving the drug-like properties for this series of compounds.

Encouragingly, as illustrated in Table 3, CF₃-containing 2-amino pyridine segment could obviously enhance the inhibitory effect against PI3K α (**29**, **32** and **33** vs **18**). In line with the previous reported, replacing the morpholine ring with other nitrogen rings



Scheme 1. Design Strategy of New PI3K Inhibitors.



Scheme 2. Synthesis of Compounds 18-23.

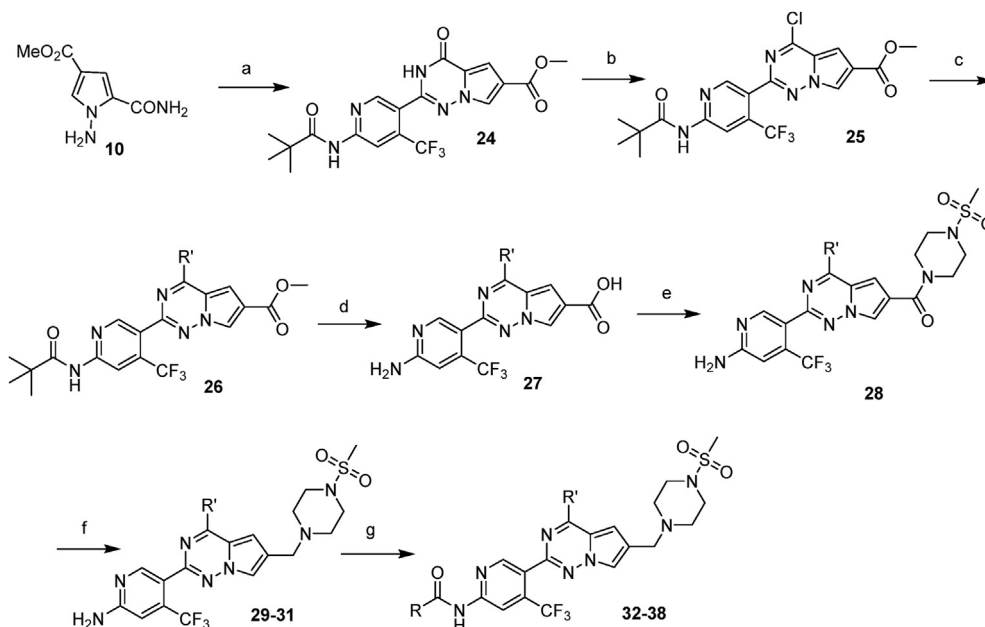
Reaction conditions: a. K_2CO_3 , NH_2Cl , dry DMF, rt, 93%; b. $NH_3/MeOH$, $100\text{ }^\circ C$ (sealed tube), 54%; c. 4-nitrobenzaldehyde, $CuCl_2 \cdot 2H_2O$, DMSO, $100\text{ }^\circ C$, 72%; d. $POCl_3$, DMAP, ref., 92%; e. morpholine, THF, ref., 94%; f. Pd/C , H_2 , MeOH, rt, 99%; g. 2 M NaOH, EtOH, ref., 69%; h. HBTU, Et_3N , amine, DMF, rt, 32%; i. $BH_3 \cdot SMe_2$, THF, ref., 55%; j. $RNCO/CH_2Cl_2$, rt, 40–49%; k. 1 M KOH, MeOH, ref., 82%; l. iPr_2NEt , amines, HBTU, dry DMF, rt, 37–39%.

caused slightly reducing activity (**30**, **31** vs **29**). Next, we continued to modify the substituents on the amino group of compound **29**, mainly because of the great versatility of this region for SAR. It was found that a wide range of substituents (compounds **32**–**35**) on the amino group were well tolerated. Although these compounds bearing a urea unit (**32**, **33**, **35**) or acrylamide (**34**) displayed excellent activity at both the enzymatic and cellular level, we suspected that their PK profiles might be a problem based on our previous study for compounds **21** and **22**. Recently, carbamates as a useful moiety to interact with drug target are specifically introduced in drug discovery [40]. Hence, compounds **36**, **37** and **38** bearing carbamate moiety were prepared and evaluated, and pleasingly the compound **37** showed the highest potency of all the synthetic compounds against PI3K α ($IC_{50} = 5.9\text{ nM}$). Despite compound **35** displayed most potent cellular inhibitory activity, its poor

oral bioavailability (7.5%) impeded it to be the best choice for further evaluation. And compound **29** also had a poor PK profile in our previous experiment (Data not shown). It is worth noting that a series of similar piperazine analogues bearing imidazo[1,2-*a*]pyridine, pyrazolo[1,5-*a*]pyridine or thieno[3,2-*d*]pyrimidine skeletons have been well established as PI3K inhibitors [32–34]. However, comparing to these previous reported inhibitors, compound **37** showed superior drug-like properties with good isoform selectivity and PK profiles.

2.4. Kinase inhibition assay of compound 37

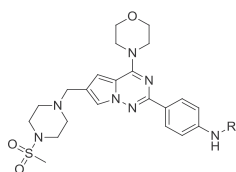
The specificity of compound **37** was further validated by being tested over 62 kinases in the KinaseProfiler panel. Compound **37** exhibited excellent selectivity for PI3Ks (Shown in Table S2 in SI). Of

**Scheme 3.** Synthesis of Compounds 28-38

Reaction conditions: a. aldehyde, $\text{CuCl}_2 \cdot 2\text{H}_2\text{O}$, DMSO, 100°C , 60%; b. POCl_3 , DMAP, reflux, 93%; c. morpholine/8-oxa-3-azabicyclo[3.2.1]octane/(S)-3-methylmorpholine, THF, reflux 60–85%; d. 2 M KOH, EtOH, reflux, 52–93%; e. HBTU, Et_3N , amines, DMF, rt, 85–94%; f. $\text{BH}_3 \cdot \text{SMe}_2$, THF, reflux, 17–57%; g. RNCO or RCOCl, CH_2Cl_2 , rt, 19–60%.

Table 1

The activity for compounds 18 and 21–23 to inhibit PI3K p110 α kinase activity and cell proliferation in tumor cells.



Compd.	R	IC ₅₀		MW	tPSA
		PI3K α (nM)	Rh30 (μM)		
18	4-FPhNHCO	105.3 \pm 24.1	0.23 \pm 0.03	608	122
21		67.5 \pm 7.9	0.09 \pm 0.01	661	142
22		41.1 \pm 4.3	0.07 \pm 0.00	716	146
23		39.6 \pm 4.3	0.08 \pm 0.01	744	155
BYL719	–	17.8 \pm 0.7	7.60 \pm 1.39	441	100
GDC-0941	–	–	0.478 \pm 0.084		

the 62 tested kinases, only c-RAF was inhibited by greater than 50% in the presence of 10 μM CYH33. Further study indicated compound

Table 2

The activity of test compounds against the proliferation of a panel of 9 NSCLC cell lines.

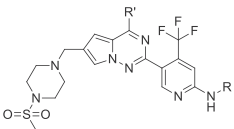
Compd.	IC ₅₀ (μM)								
	H1975	H460	Calu-3	H1650	H358	A549	H23	H266	H522
18	0.46	0.897	2.36	2.3	1.29	1.64	0.695	1.08	1.02
22	0.025	0.293	0.79	0.344	0.187	0.144	0.052	0.106	0.751
GDC-0941	0.703	1.26	2.87	4.73	1.33	2.48	0.936	5.91	2.14

37 was much less potent against c-RAF than PI3K α with an IC₅₀ around 1 μM . Thus, the compound **37** demonstrates significant selectivity for inhibition of p110/p85 over other tested kinases. Additional profiling of compound **37** demonstrated that compound **37** essentially inhibited against PI3K α but only less inhibited against PI3K β and PI3K γ (Table 4). E545K and H1047R are two hotspot mutations at PIK3CA in many types of cancer, which result in hyper-activation of PI3K α and promote tumorigenesis. We found **37** was able to inhibit these two mutants, indicating that **37** may be active in cancers harboring these two mutants. It is worth noting that no significant inhibiting activity against m-TOR was observed ($>10 \mu\text{M}$).

2.5. Molecular modelling of compound 37

To get a better idea of the potential binding modes of these inhibitors, compound **37** was also chosen for docking studies within the PI3K α crystal structure (Fig. 2) [41,42]. The result revealed that the interactions of compound **37** at the hinge part were very similar to CNX-1351, a covalent PI3K α ligand in the crystal structure 3ZIM, forming interaction between the morpholine ring and the backbone of residue Val851 through a hydrogen bond, and positioning the central scaffold at same location. Comparing to the ligand CNX-1351, compound **37** has a different functional motif of carbamate group at the back site, which interacts with side chain of residue Lys802 through a hydrogen bond. The CF_3 group on pyridine pointed upwards to the vicinity of the P-loop in the N lobe of the catalytic domain of PI3K α . The piperazine

Table 3
Inhibition of PI3K α and proliferation for compounds 29–38^a.



Compd	R'	R	IC ₅₀	
			PI3K α (nM)	Rh30 (μ M) ^b
29		H	55.4 \pm 4.2	0.88 \pm 0.08
30		H	243.8 \pm 6.3	1.78 \pm 0.02
31		H	50.5 \pm 0.04	0.97 \pm 0.07
32		4-FPhNHCO	17.7 \pm 1.3	0.18 \pm 0.02
33		EtNHCO	41.7 \pm 2.0	0.39 \pm 0.02
34		CH ₂ =CHCO	19.9 \pm 0.1	0.71 \pm 0.23
35		MeNHCO	23.6 \pm 3.3	0.15 \pm 0.03
36		EtOCO	21.0 \pm 1.4	3.27 \pm 0.20
37(CYH33)		MeOCO	5.9 \pm 1.1	1.03 \pm 0.04
38		PhOCO	44.4 \pm 4.1	5.07 \pm 0.37
BYL-719	–	–	17.8 \pm 0.7	7.60 \pm 1.39

^a The values are averages of at 3 separate determinations.

^b Cell proliferation with Rh30 cells was measured by an SRB assay.

segment extended to the solvent-accessible region, which can interact with the nearby residue Arg770 through the electrostatic force. Overall, the binding mode of compound **37** resembles the typical ATP-competitive inhibitor of PI3K α and makes enhanced interactions with the protein and results high affinity.

Table 4
Activities of 37 against class I PI3Ks and PIK3CAmutants.

Compd	IC ₅₀ (nM)					
	PI3K α wt	PI3K α E545K	PI3K α H1047R	PI3K β	PI3K γ	PI3K δ
37	5.9 \pm 1.1	17.1 \pm 3.4	8.4 \pm 2.7	598.1 \pm 147.2	224.8 \pm 50.5	78.7 \pm 4.8
BYL719	17.8 \pm 0.7	18.9 \pm 1.7	10.9 \pm 3.4	1837.3 \pm 434.2	1673.0 \pm 389.4	382.8 \pm 55.8

^aThe values are averages of at least 3 separate determinations with typical variations of less than $\pm 20\%$ Fig. 1.

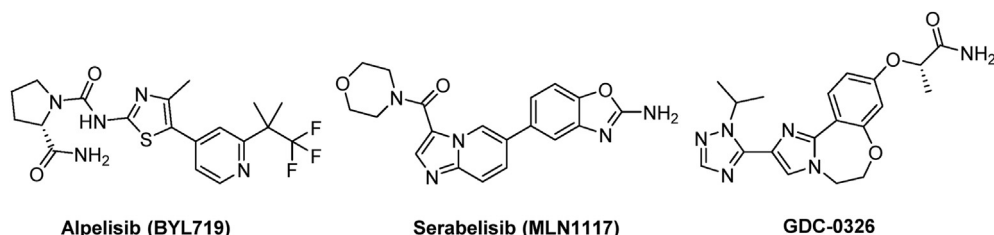


Fig. 1. Some representative structure of PI3K α inhibitors.

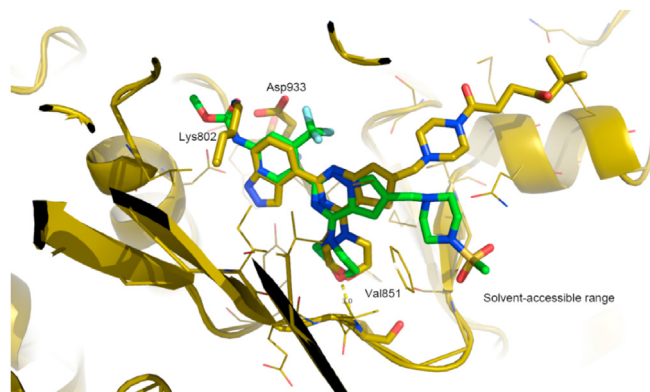


Fig. 2. Proposed binding mode for compound **37** (PDB ID: 3ZIM). Docking poses of compound **37** (green) and **CNX-1351** (brown) to key residues are labeled in stick mode. Image generated by PyMol.

2.6. Compound 37 selectively inhibited PI3K α at cellular level

Rh30-Myr-p110s isogenic cell lines previously established in our lab were employed to detect the selectivity of compound **37** among isoforms of class I PI3K. Under serum-free culture conditions, endogenous PI3K is not activated. Whereas the ectopically expressed p110 isoforms that are membrane-anchored, are constitutively active because of myristoylation at N-terminal. As shown in Fig. 3, phosphorylation of Akt in Rh30-Myr-p110 α cells was significantly inhibited by compound **37** at the concentration of 14 nM, which was comparable to the IC₅₀ against PI3K in biochemical assay. Much higher concentrations (~10 times) of compound **37** was needed to block Akt phosphorylation in p110 β -, p110 γ - or p110 δ -active Rh30 cells, demonstrating compound **37** preferentially inhibited the kinase activity of PI3K p110 α at cellular level.

2.7. Compound 37 potently inhibited PI3K signaling in tumor cells

To explore whether compound **37** is able to inhibit PI3K signaling in human tumor cells, glioblastoma U87MG and rhabdomyosarcoma Rh30 cells were exposed to compound **37** or **GDC0941** for 1 h and then stimulated with recombinant human

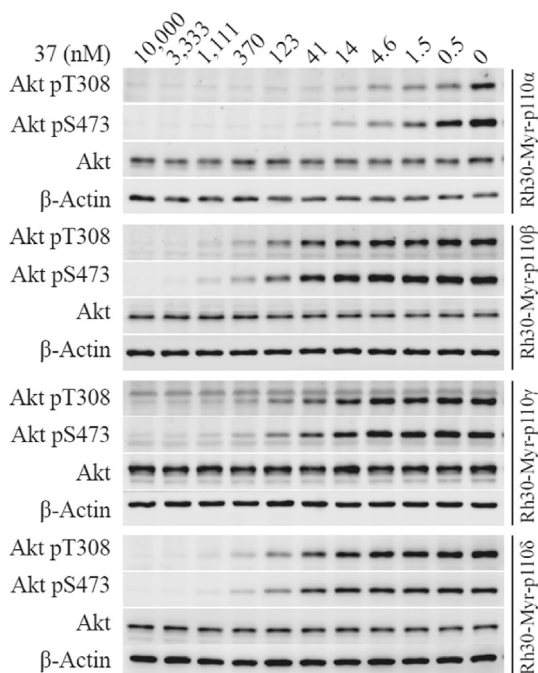


Fig. 3. Compound **37** selectively inhibited PI3K α at cellular level.

insulin-like growth factor 1 (rhIGF1) to activate IGFR-PI3K-Akt pathway. As shown in Fig. 4, compound **37** inhibited Akt phosphorylation at Ser473 and Thr308 in a concentration-dependent manner in both cell lines. The potency of compound **37** was comparable to GDC0941, a pan-PI3K inhibitor.

2.8. Compound **37** inhibited potently proliferation of a panel of tumor cells

Compound **37** was next tested for its activity to inhibit cell proliferation in a panel of 21 tumor cells originated from lung, breast, ovary and colon, prostate etc. As shown in Fig. 5, half of the tested cells were sensitive to compound **37** with IC_{50} s less than 1 μ M. It is noteworthy that most of sensitive cells were originated from breast cancer, which was consistent with the fact that PI3K is frequently hyper-activated in breast cancer. Moreover, the potency of compound **37** was comparable to **GDC0941** and the anti-proliferative profile of these two compounds was highly similar. Thus **37** had potent antitumor activity *in vitro*.

2.9. Compound **37** potently inhibited the growth of human tumor cell xenografts

To investigate whether compound **37** inhibit PI3K signaling in tumor tissue, mice bearing ovarian cancer SKOV-3 xenografts were orally administrated with 5 mg/kg compound **37** according to the preliminary PK study and tumor samples were collected 0 h, 2 h, 4 h or 8 h later. Phosphorylated Akt significantly decreased 2 h after single treatment of **37** (Fig. 6A). Partial restoration of Akt phosphorylation could be observed 4 h later and Akt phosphorylation restored to the level of control group 8 h later. The fluctuation of phosphorylated AKT reflected the half-life of compound **37** ($T_{1/2} = 1.49$ h, Table 6) in rats. As compound **37** displayed potent activity against the proliferation of SKOV-3 cells and inhibited PI3K signaling in SKOV-3 xenografts, the efficacy of **37** on the growth of SKOV-3 xenograft-bearing on nude mice was evaluated. As shown in Figs. 6B, **37** was administrated orally once a day for 21 days and significantly inhibited the growth of xenograft in a dose-dependent manner, yielding treated/control values of 67.4%, 48.1% and 37.0% at doses of 5 mg/kg, 10 mg/kg and 20 mg/kg respectively. Moreover, no significant weight loss and toxic symptoms were observed during the treatment period (Fig. 6C), suggesting the favorable safety profile of this compound.

PI3K α is very important in glucose metabolism and hyperglycemia, thus we detected the tolerance of glucose after mice bearing SKOV-3 xenografts were administrated with **37** for 18 days. As shown in Fig. 6D, no significant difference was observed between compound **37**-treated groups and vehicle control group in basal

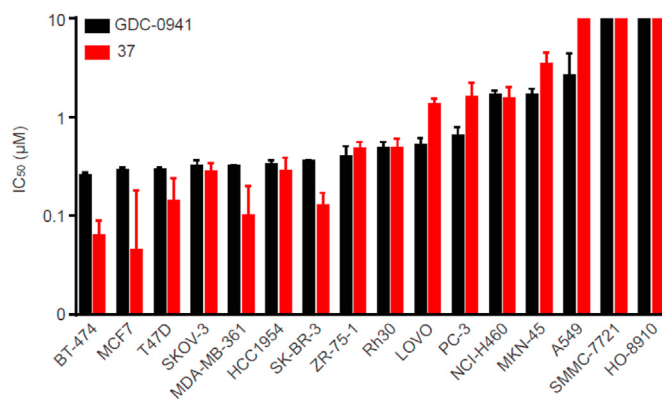


Fig. 5. Compound **37** potently inhibited proliferation of a panel of tumor cells. Cells seeded in 96-well plates were treated with test compounds for 72 h and then SRB assay was performed. The average IC_{50} values were from at least three independent tests and data were shown as mean \pm SD.

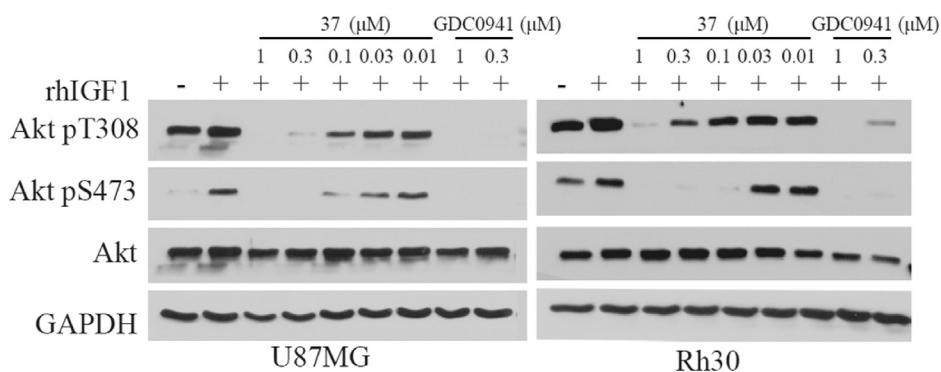


Fig. 4. Compound **37** inhibited PI3K-mediated signaling in human tumor cells. U87MG or Rh30 cells grown in 12-well plates were incubated in serum-free medium for 24 h. After exposure to **37** for 1 h, cells were stimulated with 50 ng/ml IGF-I for 10 min. Cells were then collected and subjected to standard Western blot analysis with the indicated antibodies.

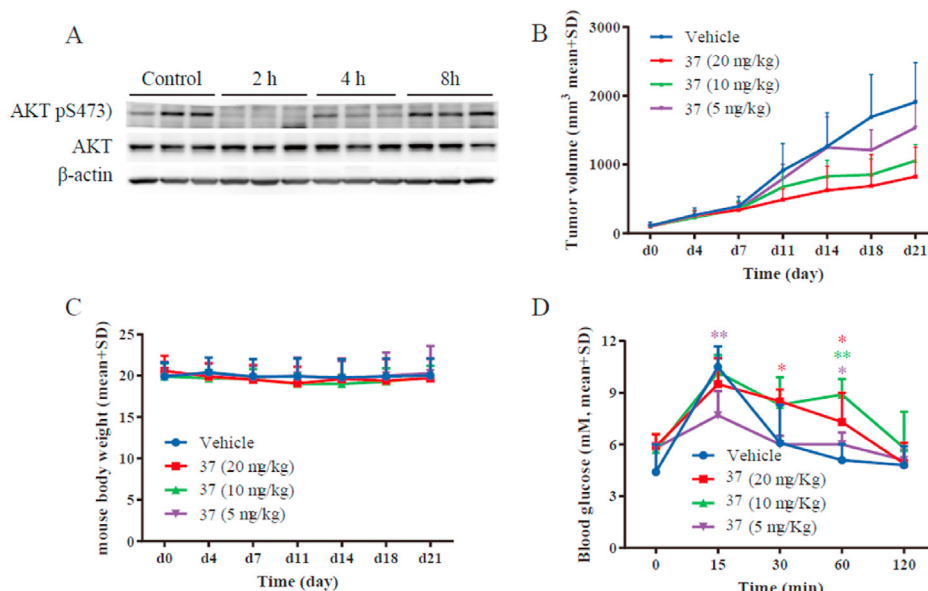


Fig. 6. **37** potentially inhibited growth of human tumor cell xenografts. (A) Mice bearing SKOV-3 xenografts were orally (P.O.) administered with vehicle control or **37** at 5 mg/kg. Tumor samples were collected at indicated times to Western blot with indicated antibodies was performed. (B) Xenograft-bearing mice were administered orally with vehicle or **37** at indicated doses once a day. The tumor volume (B) and body weight (C) were measured individually twice per week. (D) SKOV-3 xenograft bearing mice were treated with vehicle or **37** once a day for 18 days, and then subjected to glucose tolerance assay. Data were shown as mean +SD and analyzed by unpaired student's t-test. *: $p < 0.05$; **: $p < 0.01$.

Table 5
Stability of compound **37** in hepatocyte cultures.

Compd	Parameter	human	monkey	dog	rat	mouse
37	Cl_{int}^p (mL/min/Kg)	3.05	28.97	39.54	16.95	21.57
	$T_{1/2}$ [min]	407.7	43.05	87.74	147.4	93.67

level of blood glucose. In vehicle control group, the level of blood glucose of fasted mice that were fed with glucose increased but returned to normal up to 2 h. Though the treatment with compound **37** delayed the restoration of blood glucose, the levels of blood glucose on compound **37**-treated groups were similar to that of control group up to 2 h, which well indicated that the side effect of compound **37** is minor and manageable.

2.10. Preliminary PK profile of compound **37** and hERG test

Given the encouraging biological profile, metabolic stability and pharmacokinetic properties of compound **37** were also assessed. Stability of compound **37** was evaluated by the parameters in microsome assays referred to clearance and half-live measurements of the species including human, cynomolgus monkey, beagle dog, rat, and mouse. Except for human hepatocyte, moderate to high clearance was obtained for compound **37** (Table 5). The half-life of compound **37** was 6.8 h in the presence of human hepatocytes, and was 2.5 h in rat hepatocytes. *In vivo* pharmacokinetic parameters were subsequently investigated in male rats. As summarized in Table 6, the volume of distribution and plasma clearance

Table 6
PK properties of **37** in male rats.

Compd.	route	dose (mg/kg)	C_{max} (ng/mL)	T_{max} (h)	$T_{1/2}$ (h)	$AUC_{0-\infty}$ (ng•h/mL)	Cl_p (L/h/kg)	V_{ss} (L/kg)	F (%)
37	p.o.	10	831.5	0.875	1.49	2749	—	—	36.9
	i.v.	5	—	—	0.98	3559	1.44	1.843	—

were moderate. And oral bioavailability of compound **37** was acceptable (37%). Additionally, no obvious inhibitions of Cytochrome 450 isozymes ($IC_{50} > 30 \mu M$, Table S3 in SI) and the hERG K^+ channel ($IC_{50} > 40 \mu M$, patch clamp assay, Figure S1 in SI) were observed.

3. Conclusions

Structural modifications of the tricyclic lead compound **1** through scaffold hopping/contraction and pharmacophore hybridization led to new pyrrolo[2,1-*f*][1,2,4]triazines analogues as potent PI3K α inhibitors. Among these, compound **37** with improved pharmacokinetic profiles exhibited efficient inhibitory on the growth of SKOV-3 xenografts in nude mice. Western blot assay of compound **37**-treated SKOV-3 tumors showed significant decrease in pAKTS473, demonstrating that compound **37** blocked the PI3K/AKT/mTOR pathway *in vivo*. Additionally, compound **37** exhibited significant selectivity among tested protein kinases. In summary, compound **37** emerged as a new selective PI3K inhibitor exhibiting potent activity against human solid tumors with alterations in PI3K pathway and favorable pharmaceutical profile, which makes it a promising drug candidate. **CYH33** is now in phase Ib clinical trial in China and IND application has been approved by FDA in United States.

4. Experimental

4.1. Chemistry

All solvents and reagents were commercially available and used without further purification. Unless otherwise noted, all reagents were weighed and handled in air at room temperature. Chromatography was performed on silica gel (200–300 mesh). NMR spectra were recorded on Bruker Avance300/400/500 NMR spectrometer. Chemical shifts were reported in parts per million (ppm, δ). Proton coupling patterns are described as singlet (s), doublet (d), triplet (t), quartet (q) and multiplet (m). Tetramethylsilane (TMS)

was used as internal standard (^1H NMR: TMS at 0.00 ppm; CHCl_3 at 7.26 ppm; ^{13}C NMR: CDCl_3 at 77.2 ppm, DMSO at 33.5 ppm). Low and high-resolution mass spectra (LRMS and HRMS) were recorded on a Finnigan/MAT-95 (EI), Finnigan LCQ/DECA and Micromass Ultra Q-TOF (ESI) spectrometer. The purity of the final compounds was determined to be greater than 95% by HPLC analysis [HPLC: column, Eclipse XDB-C18, 4.6×150 mm, $5 \mu\text{m}$; Methanol-water (95 : 5) was used as the mobile phase for compounds **18**, **22** and **23**, 1.0 mL/min; Methanol-water with 0.1% formic acid (50:50) was used as the mobile phase for compounds **21**, **33**, **34**, **35**, **36**, and **37**, 1.0 mL/min; And the mobile phase for compounds **29**, **30**, **31**, **32**, and **38** is acetonitrile-water (80 : 20), 1.0 mL/min; UV detection at 254 nm; oven temperature, 35°C . Agilent 1200, Agilent Technologies, CA, USA].

4.2. Docking study

The crystal structure of PI3K α (PDB ID: 3ZIM) was downloaded from PDB database and used as the docking receptor model. The structure was processed with protein preparation module in Schrödinger software package, [41], and presented PI3K α inhibitor in 3ZIM was selected as the location of binding site for making the grid file with Glide module. Then the ligand **37** was prepared to add the partial charge, minimize to obtain the low-energy conformation. Finally, the ligand was docked into the grid files with default parameters at XP precision mode [42], and the predicted binding mode was depicted with Pymol software.

4.3. PI3K kinase assay

PI3-kinase HTRF Assay kit (Millipore) was used to determine the IC_{50} values of all the test compounds as instructed. Briefly, desired concentration of each enzyme was incubated in the assay buffer containing $10 \mu\text{M}$ PIP2 in a white 384-well plate (PerkinElmer). The test compounds were dissolved at 10 mM in dimethylsulfoxide (DMSO) as stock solutions, and aliquots were stored at -20°C until use. The reaction was initiated by adding ATP and then incubated at room temperature for 30 min. Subsequently, stop solution and detection mix were added to each well to terminate the reaction. The light emission intensity was measured by an EnVision Multilabel Reader (PerkinElmer). IC_{50} values were calculated by using GraphPad Prism 6 software (GraphPad Software, San Diego California USA).

4.4. Cell culture

PC-3 and A549 cells were cultured in F-12 K medium with 10% fetal bovine serum (FBS). MCF7, U87MG, MDA-MB-361 and HCT116 cells were cultured in DMEM+10% FBS, and rest of the cell lines were maintained in RPMI 1640 + 10% FBS. All cells were verified by short tandem repeat analysis and mycoplasma-free.

4.5. Cell Proliferation Assay [43].

Cell proliferation was determined with SRB (Sulforhodamine B) assay. Briefly, exponentially growing cells were seeded at a density of 3000–5000 per well in 96-well microtiter plates. After 24 h, serially diluted compounds was added to achieve desired concentration. Following 72-h culture, Cells were then fixed with 10% trichloroacetic acid and then stained with SRB (Sigma-Aldrich). The remaining SRB in the cells was dissolved in 10 mM Tris-HCl and was measured at 560 nm using a multiwell spectrophotometer. The inhibitory rate was calculated using the formula: $(\text{OD}_{\text{control cells}} - \text{OD}_{\text{treated cells}}) / \text{OD}_{\text{control cells}} \times 100\%$.

4.6. Western Blotting [44].

Tumor cells were lysed in RIPA buffer and quantified. Equal amount of protein was reconstituted in $1 \times$ SDS-loading buffer (50 mM Tris-HCl (pH 8.0), 2% SDS, 100 mM DTT, 0.001% bromophenol blue, 10% glycerol) and was heated at 95°C for 10 min. Standard Western blot was proceeded with the primary antibodies against Akt (cell signaling technology), phosphorylated Akt at T308 (cell signaling technology), phosphorylated Akt at S473 (cell signaling technology), β -Actin (Sigma-Aldrich) and GAPDH (Kang-Chen Biotech). HRP conjugated second antibody was used to generate luminescent images which were captured by ImageQuant LAS4000.

4.7. Phosphorylated Akt inhibition in xenograft

When SKOV-3 xenograft reached 200 mm^3 , mice were orally administrated (P.O.) with **37** at dose of 5 mg/kg. Tumor tissues were collected at indicated times and were then homogenized and subjected to Western blot.

4.8. Xenograft models in nude mice

4 to 5-week-old female BALB/cA nude mice (60 mice) were from Shanghai Institute of Materia Medica (SCXK(HU)2013–0017). All animals were housed in a specific pathogen-free facility and the protocol was approved by the Institutional Animal Care and Use Committee of the Shanghai Institute of Materia Medica, Chinese Academy of Sciences. The IACUC number is 2014-03-DJ-13. Human ovarian carcinoma SKOV-3 xenografts were established by inoculating 5×10^6 cells s.c. in nude mice. The experiments began when the xenografts had one passage in nude mice. Under a sterilization condition, well-grown tumors were cut into 1.5 mm^3 fragments, which were transplanted s.c. into the right flank by trocar in nude mice. When tumor reached a volume of about 100 mm^3 , the mice were randomized to treat with vehicle or compounds at indicated doses orally once a day. The animal weight and size of tumors were measured individually twice per week. Tumor volume (V) was calculated as $V = (\text{length} \times \text{width} [2]) / 2$.

4.9. Glucose tolerance assay

SKOV-3 xenograft bearing mice were treated with vehicle or compound **37** once a day for 18 days. Mice were orally administrated with glucose at 2 g/kg after being fasted for 6 h. Blood was collected immediately at indicated times and glucose concentration was tested with a blood glucose meter.

4.10. hERG test

Currents were recorded in CHO cells stably transfected with hERG channels. During recording, cells were perfused with extracellular solution containing (in mM): 145 NaCl, 5 mM KCl, 2 mM CaCl_2 , 1 mM MgCl_2 , 10 mM HEPES and 10 mM Glucose, pH 7.4 with NaOH. Electrodes (a tip resistance of 3–5 MegOhm) were pulled from borosilicate glass pipette (Sutter instrument BF150-86-10) and filled with intracellular solution contained (in mM): 140 KCl, 1 mM MgCl_2 , 0.1 mM CaCl_2 , 5 EGTA and 10 mM HEPES, pH 7.3 adjusted with KOH). Data were obtained using an EPC10 amplifier (HEKA), signals were filtered at 1 kHz and sampled at frequencies of 10 kHz using PatchMaster software. Series resistance was compensated for 60–80%. The cells were held at -80 mV and hERG potassium currents were activated by a 2s depolarization potential of $+40 \text{ mV}$ followed by a re-polarization potential of -20 mV for 2s then back to the holding potential. Experiments were performed at room

temperature. The peak amplitude of hERG current was measured and exported to Excel and GraphPad Prism 5 for subsequent analysis.

Declaration of competing interest

The authors declare that they have no known competing financial interests or personal relationships that could have appeared to influence the work reported in this paper.

Acknowledgment

This work was supported by the National Natural Science Foundation of China (90713034 and 81703365), Institutes for Drug Discovery and Development, Chinese Academy of Sciences (CASIMM0120185009), the State Key Laboratory of Drug Research Program (SIMM1705KF-15), "Personalized Medicines-Molecular Signature-based Drug Discovery and Development", Strategic Priority Research Program of the Chinese Academy of Sciences (XDA12020111, XDA12050407) and National Science and Technology Major Project "Key New Drug Creation and Manufacturing Program" (2018ZX09711002-011-014).

Appendix A. Supplementary data

Supplementary data related to this article can be found at <https://doi.org/10.1016/j.ejmech.2020.112913>.

Abbreviations

PI3K	phosphatidylinositol 3-kinases
PIP2	phosphatidylinositol 4,5-bisphosphate
PIP3	phosphatidylinositol 3,4,5-triphosphate
mTOR	The mammalian target of rapamycin
SAR	structure-activity relationship
SPR	structure-pharmacokinetic relationship
IC ₅₀	50% inhibitory concentration

References

- [1] S.J. Leever, B. Vanhaesebroeck, M.D. Waterfield, Signalling through phosphoinositide 3-kinases: the lipids take centre stage, *Curr. Opin. Cell Biol.* 11 (1999) 219–225.
- [2] D.A. Fruman, C. Rommel, PI3K and cancer: lessons, challenges and opportunities, *Nat. Rev. Drug Discov.* 13 (2014) 140–156.
- [3] K.D. Courtney, R.B. Corcoran, J.A. Engelman, The PI3K pathway as drug target in human cancer, *J. Clin. Oncol.* 28 (2010) 1075–1083.
- [4] I. Vivanco, C.L. Sawyers, The phosphatidylinositol 3-Kinase AKT pathway in human cancer, *Nat. Rev. Canc.* 2 (2002) 489–501.
- [5] J.A. Engelman, Targeting PI3K signalling in cancer: opportunities, challenges and limitations, *Nat. Rev. Canc.* 9 (2009) 550–562.
- [6] J. Yang, J. Nie, X. Ma, Y. Wei, Y. Peng, X. Wei, Targeting PI3K in cancer: mechanisms and advances in clinical trials, *Mol. Canc.* 18 (2019) 26.
- [7] M. Sun, P. Hillmann, B.T. Hofmann, J.R. Hart, P.K. Vogt, Cancer-derived mutations in the regulatory subunit p85alpha of phosphoinositide 3-kinase function through the catalytic subunit p110alpha, *Proc. Natl. Acad. Sci. Unit. States Am.* 107 (2010) 15547–15552.
- [8] N. Vasan, P. Razavi, J.L. Johnson, H. Shao, H. Shah, A. Antoine, et al., Double PIK3CA mutations in cis increase oncogenicity and sensitivity to PI3Kalpha inhibitors, *Science* 366 (2019) 714–723.
- [9] X. Wang, J. Ding, L.H. Meng, PI3K isoform-selective inhibitors: next-generation targeted cancer therapies, *Acta Pharmacol. Sin.* 36 (2015) 1170–1176.
- [10] A.E. Garces, M.J. Stocks, Class I PI3K clinical candidates and recent inhibitor design strategies: a medicinal chemistry perspective, *J. Med. Chem.* 62 (2019) 4815–4850.
- [11] M.S. Miller, P.E. Thompson, S. Gabelli, Structural determinants of isoform selectivity in PI3K inhibitors, *Biomolecules* 9 (2019) 82.
- [12] W. Zhao, Y. Qiu, D. Kong, Class I phosphatidylinositol 3-kinase inhibitors for cancer therapy, *Acta Pharm. Sin.* B 7 (2017) 27–37.
- [13] Y. Jeong, D. Kwon, S. Hong, Selective and potent small-molecule inhibitors of PI3Ks, *Future Med. Chem.* 6 (2014) 737–756.
- [14] C. Fritsch, A. Huang, C. Chatenay-Rivauday, C. Schnell, A. Reddy, M. Liu, et al., Characterization of the novel and specific PI3Kalpha inhibitor NVP-BYL719 and development of the patient stratification strategy for clinical trials, *Mol. Canc. Therapeut.* 13 (2014) 1117–1129.
- [15] L. So, S.S. Yea, J.S. Oak, M. Lu, A. Manmadhan, Q.H. Ke, et al., Selective inhibition of phosphoinositide 3-kinase p110 α preserves lymphocyte function, *J. Biol. Chem.* 288 (2013) 5718–5731.
- [16] T.P. Heffron, R.A. Heald, C. Ndubaku, B. Wei, M. Augustin, S. Do, et al., The rational design of selective benzoxazepin inhibitors of the α -isoform of phosphoinositide 3-kinase culminating in the identification of (S)-2-((2-(1-isopropyl-1H-1,2,4-triazol-5-yl)-5,6-dihydrobenzo[f]imidazo[1,2-d][1,4]oxazepin-9-yl)oxy)propanamide (GDC-0326), *J. Med. Chem.* 59 (2016) 985–1002.
- [17] Y. Yin, S. Sha, X. Wu, S.F. Wang, F. Qiao, Z.C. Song, et al., Development of novel chromeno[4,3-c]pyrazol-4(2H)-one derivatives bearing sulfonylpiperazine as antitumor inhibitors targeting PI3Kalpha, *Eur. J. Med. Chem.* 182 (2019) 111630.
- [18] Y. Yin, J.Q. Hu, X. Wu, S. Sha, S.-F. Wang, F. Qiao, et al., Design, synthesis and biological evaluation of novel chromeno 4,3-c pyrazol-4(2H)-one derivatives containing sulfonamido as potential PI3K alpha inhibitors, *Bioorg. Med. Chem.* 27 (2019) 2261–2267.
- [19] H.W. Ding, S. Wang, X.C. Qin, J. Wang, H.R. Song, Q.C. Zhao, et al., Design, synthesis, and biological evaluation of some novel 4-aminoquinazolines as Pan-PI3K inhibitors, *Bioorg. Med. Chem.* 27 (2019) 2729–2740.
- [20] C.R. McNamara, A. Degterev, Small-molecule inhibitors of the PI3K signaling network, *Future Med. Chem.* 3 (2011) 549–565.
- [21] S. Lin, J. Jin, Y. Liu, H. Tian, Y. Zhang, R. Fu, et al., Discovery of 4-methylquinazoline based PI3K inhibitors for the potential treatment of idiopathic pulmonary fibrosis, *J. Med. Chem.* 62 (2019) 8873–8879.
- [22] Y.N. Yu, Y. Han, F. Zhang, Z. Gao, T. Zhu, S. Dong, et al., Design, synthesis, and biological evaluation of imidazo[1,2-a]pyridine derivatives as novel PI3K/mTOR dual inhibitors, *J. Med. Chem.* 63 (2020) 3028–3046.
- [23] J. Chandrasekhar, R. Dick, J.V. Veldhuizen, D. Koditek, E.I. Lepist, M.E. McGrath, et al., Atropisomerism by design: discovery of a selective and stable phosphoinositide 3-kinase (PI3K) β inhibitor, *J. Med. Chem.* 61 (2018) 6858–6868.
- [24] M. Zhan, Y. Deng, L. Zhao, G. Yan, F. Wang, Y. Tian, et al., Design, synthesis, and biological evaluation of dimorpholine substituted thienopyrimidines as potential class I PI3K/mTOR dual inhibitors, *J. Med. Chem.* 60 (2017) 4023–4035.
- [25] J.E. Kurtz, I. Ray-Coquard, PI3 kinase inhibitors in the clinic: an update, *Anticancer Res.* 32 (2012) 2463–2470.
- [26] N. Pemberton, M. Mogemark, S. Arlbrandt, P. Bold, R.J. Cox, C. Gardelli, et al., Discovery of highly isoform selective orally bioavailable phosphoinositide 3-kinase (PI3K)- γ inhibitors, *J. Med. Chem.* 61 (2018) 5435–5441.
- [27] F.M. Elmenier, D.S. Lasheen, K.A.M. Abouzid, Phosphatidylinositol 3 kinase (PI3K) inhibitors as new weapon to combat cancer, *Eur. J. Med. Chem.* 183 (2019) 111718.
- [28] K. Kojima, M. Shimanuki, M. Shikami, I.J. Samudio, V. Ruvolo, P. Corn, et al., The dual PI3 kinase/mTOR inhibitor PI-103 prevents p53 induction by Mdm2 inhibition but enhances p53-mediated mitochondrial apoptosis in p53 wild-type AML, *Leukemia* 22 (2008) 1728–1736.
- [29] J. Wang, X. Wang, Y. Chen, S. Chen, G. Chen, L. Tong, et al., Discovery and bioactivity of 4-(2-arylpyrido[3,2':3,4]pyrrolo[1,2-f][1,2,4]triazin-4-yl) morpholine derivatives as novel PI3K inhibitors, *Bioorg. Med. Chem. Lett* 2 (2012) 339–342.
- [30] A.J. Folkes, K. Ahmadi, W.K. Alderton, S. Alix, S.J. Baker, G. Box, et al., The identification of 2-(1H-Indazol-4-yl)-6-(4-methanesulfonyl-piperazin-1-ylmethyl)-4-morpholin-4-yl-thieno[3,2-d]pyrimidine (GDC-0941) as a potent, selective, orally bioavailable inhibitor of class I PI3 kinase for the treatment of cancer, *J. Med. Chem.* 51 (2008) 5522–5532.
- [31] T.P. Heffron, M. Berry, G. Castanedo, C. Chang, I. Chuckowree, J. Dotson, et al., Identification of GNE-477, a potent and efficacious dual PI3K/mTOR inhibitor, *Bioorg. Med. Chem. Lett* 20 (2010) 2408–2411.
- [32] M. Méndez-Pertuz, M. Martínez, C. Blanco-Aparicio, E. Gómez-Casero, A.B. García, J. Martínez-Torrecuadrada, et al., Modulation of telomere protection by the PI3K/AKT pathway, *Nat. Commun.* 8 (2017) 1278.
- [33] J. Verheijen, K. Yu, L. Toral-Barza, I. Hollander, A. Zask, Discovery of 2-arylthieno[3,2-d]pyrimidines containing 8-oxa-3-azabicyclo[3.2.1]octane in the 4-position as potent inhibitors of mTOR with selectivity over PI3K, *Bioorg. Med. Chem. Lett* 20 (2010) 375–379.
- [34] I. Aragonese-Fenoll, M. Montes-Casado, G. Ojeda, Y.Y. Acosta, J. Herranz, C. Martínez, et al., ETP-46321, a dual p110 α /class IA phosphoinositide 3-kinase inhibitor modulates T lymphocyte activation and collagen-induced arthritis, *Biochem. Pharmacol.* 106 (2016) 56–69.
- [35] S. Purser, P.R. Moore, S. Swallow, V. Gouverneur, Fluorine in medicinal chemistry, *Chem. Soc. Rev.* 37 (2008) 320–330.
- [36] J. Wang, M. Sanchez-Rosello, J.L. Acena, C. del Pozo, A.E. Sorochinsky, S. Fustero, et al., Fluorine in pharmaceutical industry: fluorine-containing drugs introduced to the market in the last decade (2001–2011), *Chem. Rev.* 114 (2014) 2432–2506.
- [37] J. Rodon, I. Braña, L.L. Siu, M.J. De Jonge, N. Homji, D. Mills, et al., Phase I dose-escalation and -expansion study of buparlisib (BKM120), an oral pan-Class I PI3K inhibitor, in patients with advanced solid tumors, *Invest. N. Drugs* 32 (2014) 670–681.
- [38] D. Rageot, T. Bohnacker, E. Keles, J.A. McPhail, R.M. Hoffmann, A. Melone, et al., (S)-4-(Difluoromethyl)-5-(4-(3-methylmorpholino)-6-morpholino-1,3,5-triazin-2-yl)pyridin-2-amine (PQR530), a potent, orally bioavailable, and brain-penetrable dual inhibitor of class I PI3K and mTOR kinase, *J. Med. Chem.* 62 (2019) 6241–6261.
- [39] Y. Chen, H. Xiang, C. Tan, Y. Xie, C. Yang, A tandem copper (II)-promoted

- synthesis of 2-substituted pyrrolo[2,1-f][1,2,4] triazin-4(3H)-ones, *Tetrahedron* 69 (2013) 2714–2719.
- [40] A.K. Ghosh, M. Brindisi, Organic carbamates in drug design and medicinal chemistry, *J. Med. Chem.* 58 (2015), 2895–40.
- [41] R.A. Friesner, J.L. Banks, R.B. Murphy, T.A. Halgren, J.J. Klicic, D.T. Mainz, et al., Glide: A new approach for rapid, accurate docking and scoring. 1. Method and assessment of docking accuracy, *J. Med. Chem.* 47 (2004) 1739–1749.
- [42] R.A. Friesner, R.B. Murphy, M.P. Repasky, L.L. Frye, J.R. Greenwood, T.A. Halgren, et al., Extra precision Glide: docking and scoring incorporating a model of hydrophobic enclosure for Protein–Ligand complexes, *J. Med. Chem.* 49 (2006) 6177–6196.
- [43] X. Li, L.J. Tong, J. Ding, L.H. Meng, Systematic combination screening reveals synergism between rapamycin and sunitinib against human lung cancer, *Canc. Lett.* 342 (2014) 159–166.
- [44] J.J. Shi, S.M. Chen, C.L. Guo, Y.X. Li, J. Ding, L.H. Meng, The mTOR inhibitor AZD8055 overcomes tamoxifen resistance in breast cancer cells by down-regulating HSPB8, *Acta Pharmacol. Sin.* 39 (2018) 1338–1346.